JACS
JOURNAL OF THE AMERICAN CHEMICAL SOCIETY
Article
pubs.acs.org/JACS

Triggering the Generation of an Iron(IV)-Oxo Compound and Its Reactivity toward Sulfides by Ru^{II} Photocatalysis

Anna Company,*[,†] Gerard Sabenya,[†] María González-Béjar,[‡] Laura Gómez,[†] Martin Clémancey,[§] Geneviève Blondin,[§] Andrew J. Jasniewski,[⊥] Mayank Puri,[⊥] Wesley R. Browne,[¶] Jean-Marc Latour,[§] Lawrence Que, Jr.,[⊥] Miquel Costas,*[,†] Julia Pérez-Prieto,*[,‡] and Julio Lloret-Fillol*[,†]

[†]Grup de Química Bioinorgànica i Supramolecular (QBIS), Institut de Química Computacional i Catàlisi (IQCC) and Departament de Química, Universitat de Girona, Campus Montilivi, E17071 Girona, Catalonia, Spain

[‡]Instituto de Ciencia Molecular (ICMol), Universidad de Valencia, C/Catedrático José Beltrán 2, Paterna, E46980 Valencia, Spain

[§]CNRS, UMR 5249; CEA, DSV, iRTSV; and Laboratoire de Chimie et Biologie des Métaux; Université Grenoble Alpes, LCBM, F-38054, Grenoble, France

[⊥]Department of Chemistry and Center for Metals in Biocatalysis, University of Minnesota, Minneapolis, Minnesota 55455, United States

[¶]Stratingh Institute for Chemistry, University of Groningen, Nijenborgh 4, 9747 AG, Groningen, The Netherlands

Supporting Information

ABSTRACT: The preparation of $[Fe^{IV}(O)(MePy_2tacn)]^{2+}$ (**2**, $MePy_2tacn$ = *N*-methyl-*N*,*N*-bis(2-picolyl)-1,4,7-triazacyclononane) by reaction of $[Fe^{II}(MePy_2tacn)(solvent)]^{2+}$ (**1**) and PhIO in CH_3CN and its full characterization are described. This compound can also be prepared photochemically from its iron(II) precursor by irradiation at 447 nm in the presence of catalytic amounts of $[Ru^{II}(bpy)_3]^{2+}$ as photosensitizer and a sacrificial electron acceptor ($Na_2S_2O_8$). Remarkably, the rate of the reaction of the photochemically prepared compound **2** toward sulfides increases 150-fold under irradiation, and **2** is partially regenerated after the sulfide has been consumed; hence, the process can be repeated several times. The origin of this rate enhancement has been established by studying the reaction of chemically generated compound **2** with sulfides under different conditions, which demonstrated that both light and $[Ru^{II}(bpy)_3]^{2+}$ are necessary for the observed increase in the reaction rate. A combination of nanosecond time-resolved absorption spectroscopy with laser pulse excitation and other mechanistic studies has led to the conclusion that an electron transfer mechanism is the most plausible explanation for the observed rate enhancement. According to this mechanism, the in-situ-generated $[Ru^{III}(bpy)_3]^{3+}$ oxidizes the sulfide to form the corresponding radical cation, which is eventually oxidized by **2** to the corresponding sulfoxide.

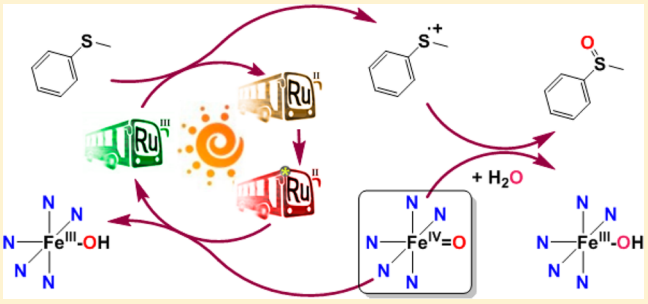

INTRODUCTION

High-valent nonheme iron-oxo species are implicated as key oxidants in the catalytic cycles of nonheme O_2-activating enzymes,[1] catalytic oxidation of inert C−H bonds,[2−5] and water oxidation to dioxygen.[6,7] Mononuclear iron(IV)-oxo intermediates have been detected and spectroscopically characterized as active oxidants in α-ketoglutarate-dependent taurine dioxygenase (TauD),[8,9] tyrosine hydroxylase, pterin-dependent phenylalanine hydroxylase, and nonheme iron-dependent halogenases.[10−12] In parallel with their discovery in biological systems, a number of synthetic iron(IV)-oxo species have been prepared.[13−15] The spectroscopic and structural properties of synthetic iron(IV)-oxo species have been analyzed in detail, and their oxidizing abilities have been a matter of intense studies.[16−21] Although some of these compounds are sufficiently powerful oxidants to oxidize even the strong C−H bonds of cyclohexane,[16] their reactivity is far less than the extraordinary activity exhibited by enzymes.[22,23] The factors that determine the reactivity of the oxoiron(IV) unit are of central interest, and extensive efforts have been directed toward the use of coordination complexes as synthetic models.

The use of oxygen atom donors such as iodosobenzene (PhIO) is the most common strategy for the chemical synthesis of model iron(IV)-oxo species.[24] Less common is their generation using water as the oxygen source. In this regard, Nam and co-workers recently reported the generation of $[Fe^{IV}(O)(N4Py)]^{2+}$ (N4Py = *N*,*N*-bis(2-pyridylmethyl)-*N*-bis-(2-pyridyl)methylamine) from $[Fe^{II}(N4Py)(CH_3CN)](OTf)_2$ (OTf = trifluoromethanesulfonate anion) using either a strong oxidant (cerium(IV) ammonium nitrate, CAN)[25] or a photochemically generated oxidant.[26] In particular, it was reported

Received: December 3, 2013
Published: February 25, 2014

   dx.doi.org/10.1021/ja412059c | J. Am. Chem. Soc. 2014, 136, 4624−4633

Scheme 1. (a) Chemical and Photochemical Strategies for the Generation of $[Fe^{IV}(O)(MePy_2tacn)]^{2+}$ (2) from $[Fe^{II}(MePy_2tacn)(S)]^{2+}$ (1) and (b) Structure of the Previously Reported $[Fe^{IV}(O)(Me_2Py_2tacn)]^{2+}$ (3)[27]

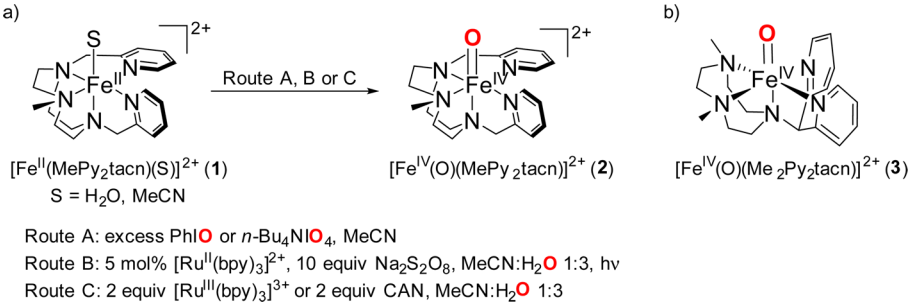

that $[Ru^{II}(bpy)_3]^{2+}$ could be used as a photosensitizer in combination with $[Co^{III}Cl(NH_3)_5]^{2+}$ as the terminal electron acceptor to generate the iron(IV)-oxo compound.

Herein, we show that the new complex $[Fe^{IV}(O)(MePy_2tacn)]^{2+}$ (**2**, $MePy_2tacn$ = *N*-methyl-*N*′,*N*″-bis(2-pyridylmethyl)-1,4,7-triazacyclononane, Scheme 1) can be generated from $[Fe^{II}(MePy_2tacn)(S)]^{2+}$ (**1**, S = solvent) by reaction with oxygen atom transfer oxidants (PhIO or n-Bu_4NIO_4) in CH_3CN or by using water as the source of oxygen in combination with $1e^-$ oxidants (CAN or $[Ru^{III}(bpy)_3]^{3+}$) (Scheme 1). The transformation of **1** to **2** can also be photocatalyzed by $[Ru^{II}(bpy)_3]^{2+}$ in the presence of $Na_2S_2O_8$. Importantly, the oxygen-atom transferability of the low-spin (S = 1) iron(IV)-oxo complex **2** is enhanced upon irradiation at 447 nm in the presence of $[Ru^{II}(bpy)_3]^{2+}$. The origin of this rate enhancement is investigated through nanosecond-time-resolved absorption spectroscopy.

RESULTS AND DISCUSSION

Synthesis and Characterization of $[Fe^{II}(MePy_2tacn)(CH_3CN)](OTf)_2$ (1). Reaction of the pentadentate ligand $MePy_2tacn$ (Figure 1) with an equimolar amount of $[Fe(OTf)_2(CH_3CN)_2]$ in THF under anaerobic conditions afforded $[Fe^{II}(MePy_2tacn)(CH_3CN)](OTf)_2$ (**1**) as a deep red solid. Slow diffusion of diethyl ether over a saturated CH_2Cl_2/CH_3CN solution yielded dark red crystals of **1** in 60% yield. X-ray analysis revealed a ferrous center octahedrally coordinated to the five nitrogen atoms of the ligand and to one exogenous acetonitrile molecule (Figure 1, see Supporting Information (SI) for crystallographic details). The two pyridine moieties are arranged perpendicular to one another. The average Fe−N distance is 1.98 Å, indicative of a low spin iron(II) center (S = 0).[28−30] Accordingly, a diamagnetic ^{1}H NMR spectrum is obtained for **1** in acetonitrile-d_3, indicating that the low-spin structure is retained in solution (SI Figure S1), and its Mössbauer spectrum exhibited an isomer shift (δ = 0.44 mm·s^{-1}) and a quadrupole splitting ($|\Delta E_Q|$ = 0.41 mm·s^{-1}) characteristic of a low-spin iron(II) center (SI Figure S2, Table S5).

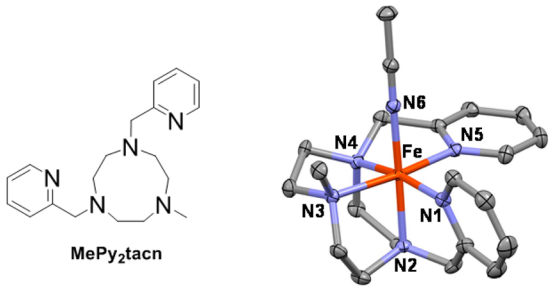

Figure 1. Left: Schematic representation of ligand $MePy_2tacn$. Right: thermal ellipsoid plot (50% probability) of **1**. Hydrogen atoms and triflate counterions have been omitted for clarity.

Chemical and Photochemical Synthesis of the Iron-(IV)-Oxo Complex 2 and Its Characterization. Iron(IV)-oxo compound **2** was obtained by direct oxidation of **1** with excess PhIO or 1.2 equiv of n-Bu_4NIO_4 in CH_3CN, as previously reported for structurally related iron(IV)-oxo compounds (route A, Scheme 1a).[15,24] The UV/vis absorption spectrum of **2** in CH_3CN (Figure 2 top) is characterized by an absorption band with a maximum at 736 nm (ε = 310 M^{-1} cm^{-1}), a common feature in S = 1 iron(IV)-oxo species.[14,15,24] Complex **2** was further characterized by Mössbauer spectroscopy using ^{57}Fe-enriched samples. As shown in Figure 3, the spectrum recorded at 80 K under zero-applied magnetic field is the superposition of two doublets. The minor one constitutes 18% of the sample (isomer shift δ = 0.48 mm·s^{-1}, quadrupole splitting ΔE_Q = 1.57 mm·s^{-1}), and it is attributed to an oxo-bridged diferric decomposition product that frequently constitutes a thermodynamic sink for the present chemistry.[17,31] The major one, corresponding to **2**, represents 82% of the total iron content and exhibits parameters (δ = −0.01 mm·s^{-1} and ΔE_Q = 0.93 mm·s^{-1}) that are consistent with an iron(IV) center in a low spin (S = 1) configuration. Electrospray ionization mass spectrometry (ESI-MS) of **2** in acetonitrile showed a single major peak at m/z 546.12, with an isotopic pattern that corresponds to $\{[Fe^{IV}(O)(MePy_2tacn)](OTf)\}^+$ (Figure 2, bottom). Furthermore, this peak shifted by two m/z units when $H_2{}^{18}O$ was added to **2**, thus further confirming the presence of an oxo ligand that readily exchanges with water. The ^{1}H NMR spectrum of **2** in CD_3CN shows paramagnetically shifted signals and resembles the structurally related iron(IV)-oxo species $[Fe^{IV}(O)(N4Py)]^{2+}$ and $[Fe^{IV}(O)(Bntpen)]^{2+}$ (Bntpen = *N*-benzyl-*N*,*N*′,*N*′-tris(2-pyridylmethyl)-1,2-diaminoethane), the signals of the pyridine moiety being the most distinctive feature (SI Figure S7).[32] A ^{1}H NMR COSY experiment shows two distinguishable sets of signals exhibiting particular shift patterns (SI Figure S8): one set corresponds to a pyridine ring placed perpendicular to the Fe=O bond (11, 2, −1 ppm), and the other set, to the pyridine ring parallel to the Fe=O axis (47, 13, −13 ppm), assigned by comparison with previous studies.[32]

X-ray absorption spectroscopy (XAS) provided insight into the structure of **2**, which was compared with those of related complexes supported by pentadentate ligands, including **3** (Scheme 1b), $[Fe^{IV}(O)(N4Py)]^{2+}$ and $[Fe^{IV}(O)(Bntpen)]^{2+}$.[27]

dx.doi.org/10.1021/ja412059c | J. Am. Chem. Soc. 2014, 136, 4624−4633

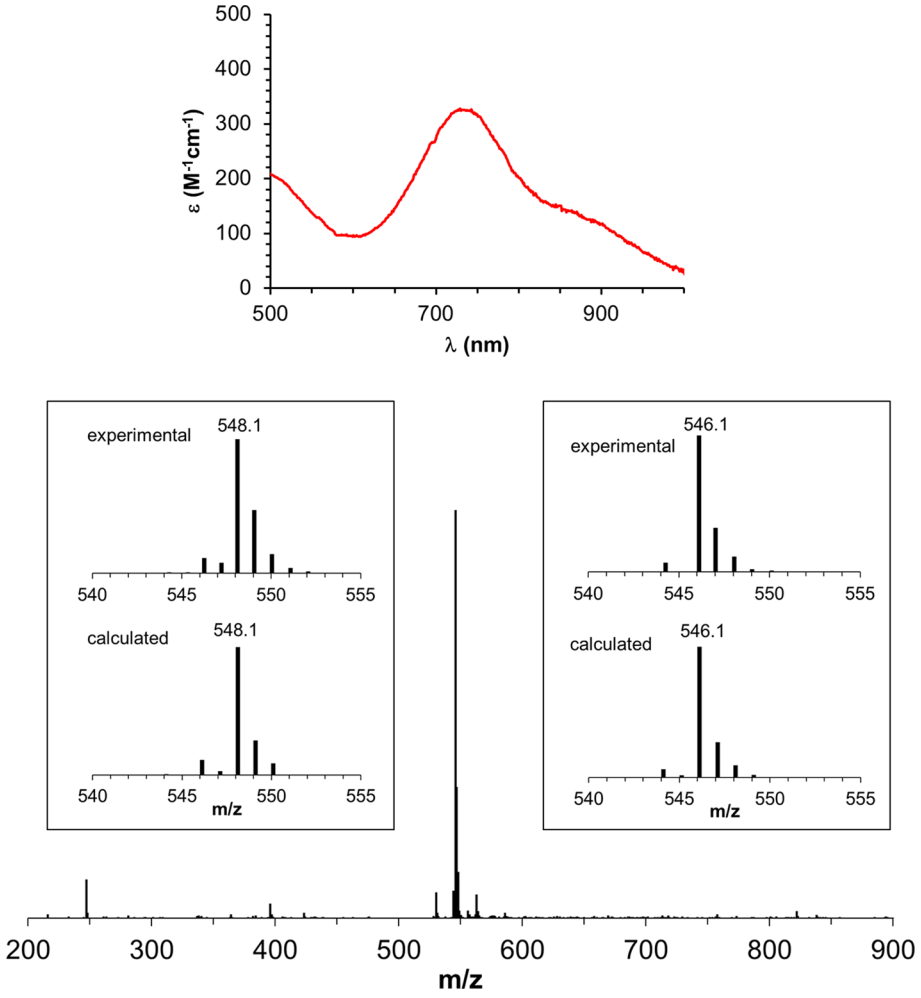

Figure 2. Top: UV/vis spectrum of **2** in CH_3CN. The extinction coefficient was determined according to the purity of the sample measured by Mössbauer spectroscopy (82%). Bottom: ESI-MS spectrum of **2** exhibiting a base peak at *m/z* 546.1. Inset right: experimental and simulated peak at *m/z* 546.1 corresponding to $\{[Fe^{IV}(O)(MePy_2tacn)](OTf)\}^+$. Inset left: experimental and simulated peak at *m/z* 548.1 corresponding to $\{[Fe^{IV}(^{18}O)(MePy_2tacn)](OTf)\}^+$ obtained after reaction of **2** with 1000 equiv $H_2{}^{18}O$. For the latter, the slight mismatch between the experimental and the calculated mass spectrum is due to the formation of iron(III)-hydroxo species as a byproduct under the experimental conditions (*m/z* 549.1 $\{[Fe^{III}(^{18}OH)(MePy_2tacn)](OTf)\}^+$).

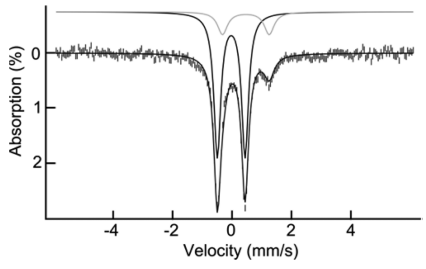

Figure 3. Mössbauer spectrum of **2** recorded at 80 K. The experimental data are the hatched bars, and the dark and light gray lines represent the contributions of **2** and a decomposition diferric product, respectively.

The rising Fe K-edge energy for **2** was found to be at 7124.2 eV and is comparable to the corresponding values measured for **3**, $[Fe^{IV}(O)(N4Py)]^{2+}$, and $[Fe^{IV}(O)(Bntpen)]^{2+}$ at 7124.7, 7124.0, and 7123.7 eV, respectively.[27] As expected, a 1s → 3d transition can be observed at 7114.1 eV in the near-edge region. The normalized area of the pre-edge peak for **2** was found to be 26 units, compared with pre-edge areas of 29−31 units for **3**, $[Fe^{IV}(O)(N4Py)]^{2+}$, and $[Fe^{IV}(O)(Bntpen)]^{2+}$, suggesting that the ligand environment of **2** is slightly less distorted than the others. Analysis of the extended X-ray absorption fine structure (EXAFS) data (Figure 4, SI Table S4)

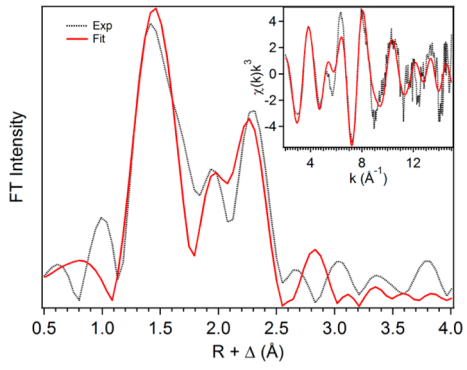

Figure 4. Best fit (red solid line) to the experimental (black dashed line) unfiltered EXAFS data (inset) and corresponding Fourier transform of **2**. *k* range = 2−15 $Å^{-1}$; back-transform range, ∼0.83−3.0 Å.

dx.doi.org/10.1021/ja412059c | J. Am. Chem. Soc. 2014, 136, 4624−4633

shows that **2** has a single O scatterer at 1.63 Å corresponding to the oxo group and a shell of nitrogen scatterers at 2.00 Å arising from the pentadentate supporting ligand, similar to the data obtained for **3**.[27] Interestingly, fitting of the outer sphere region of **2** required the inclusion of two shells of carbon scatterers at 2.81 and 2.95 Å, in contrast to **3**, for which a single shell of carbon scatterers at 2.90 Å was sufficient to fit the data. This difference likely arises from the fact that the two pyridine rings of the $MePy_2tacn$ ligand in **2** are coordinated to the iron center in somewhat different modes, as highlighted by the ^1H NMR COSY experiment (SI Figure S8). Thus, the XAS data is consistent with the structure of **2** shown in Scheme 1. Taken together, the spectroscopic data support the formulation of **2** as an $S = 1$ iron(IV)-oxo compound with the general formula $[Fe^{IV}(O)(MePy_2tacn)]^{2+}$.

Inspired by the recently described photochemical method for the generation of $[Fe^{IV}(O)(N4Py)]^{2+}$,[26] we explored the photocatalytic generation of **2** (route B, Scheme 1a). Irradiation with visible light ($\lambda_{LED} = 447 \pm 20$ nm) of a solution containing **1** (0.4 mM), 5 mol % $[Ru^{II}(bpy)_3]Cl_2$ (0.02 mM), and 10 equiv of $Na_2S_2O_8$ (4 mM) under a N_2 atmosphere at 25 °C in CH_3CN/H_2O (1:3 v/v) resulted in immediate changes in the UV/vis absorption spectrum of the reaction mixture (Figure 5).

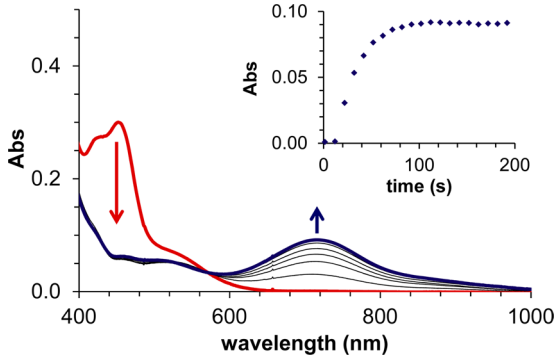

Figure 5. UV/vis absorption spectra obtained before and during irradiation (447 nm) of a sample containing **1** (0.4 mM), $[Ru^{II}(bpy)_3]Cl_2$ (0.02 mM), and 10 equiv of $Na_2S_2O_8$ (4 mM) in CH_3CN/H_2O (1:3 v/v). Inset: kinetic trace at 715 nm.

On one hand, the instantaneous oxidation of $[Ru^{II}(bpy)_3]^{2+}$ into $[Ru^{III}(bpy)_3]^{3+}$ is evidenced by the immediate disappearance of the absorption band of $[Ru^{II}(bpy)_3]^{2+}$ at 450 nm.[33] In addition, formation of **2** under these photocatalytic conditions was clearly indicated by the progressive growth within 100 s of its characteristic absorption band now centered at 715 nm (ε = 240 M^{-1} cm^{-1}; no correction was applied for the calculation of the ε value in this solvent mixture). The 20-nm shift of the λ_{max} of **2** in CH_3CN/H_2O 1:3 with respect to CH_3CN (Figure 2, top) is due to a solvatochromic effect. Such dependence of the λ_{max} on the solvent is also observed for other iron(IV)-oxo compounds, such as **3**, $[Fe^{IV}(O)(N4Py)]^{2+}$ and $[Fe^{IV}(O)(Bntpen)]^{2+}$, for which a blue shift of the d–d band of ~10 nm is observed under the same conditions. Control experiments showed that compound **2** was not formed in the absence of $[Ru^{II}(bpy)_3]Cl_2$ or $Na_2S_2O_8$.

In the absence of compound **1** and under irradiation, $[Ru^{II}(bpy)_3]^{2+}$ underwent oxidation by $Na_2S_2O_8$ to $[Ru^{III}(bpy)_3]^{3+}$, as manifested by the rapid decrease in the absorption band at λ = 450 nm and formation of the characteristic weak absorption bands of Ru^{III} around 650 nm (SI Figure S9, left). The ability of $[Ru^{III}(bpy)_3]^{3+}$ to achieve the 2-electron oxidation of **1** to **2** was proven by the stoichiometric reaction of **1** with 2 equiv of isolated $[Ru^{III}(bpy)_3]^{3+}$ (route C, Scheme 1a), which provided full conversion to **2** (SI Figure S10, left). The use of another $1e^-$ oxidant, such as cerium(IV) ammonium nitrate, also produced compound **2** (SI Figure S10, right).

These experimental data are in accordance with the mechanism depicted in Scheme 2, earlier proposed by Nam and Fukuzumi for the photochemical preparation of the iron(IV)-oxo compound $[Fe^{IV}(O)(N4Py)]^{2+}$.[26] $Na_2S_2O_8$ itself oxidizes the starting iron(II) complex (**1**) to iron(III), as clearly observed by the disappearance of the characteristic 414 nm absorption band of **1** when $Na_2S_2O_8$ is added and the appearance of the characteristic absorption bands of $[Fe^{III}(OH)(MePy_2tacn)]^{2+}$ (SI Figure S9 right and Table S5). Accordingly, the measured redox potential of the Fe^{II}/Fe^{III}–OH couple was 0.38 V vs SCE in CH_3CN/H_2O 1:3 (SI Figures S5 and S6). Further confirmation of the nature of this iron(III)-hydroxo complex was gained by Mössbauer and EPR spectroscopies (SI Figures S3 and S4, Tables S3 and S5). Direct electron transfer from the iron(III) center to $[Ru^{III}(bpy)_3]^{3+}$ gives **2** together with the corresponding one-electron-reduced Ru^{II} complex. In turn, the sacrificial electron acceptor, $Na_2S_2O_8$, regenerates $[Ru^{III}(bpy)_3]^{3+}$ by one-electron oxidation of the $*[Ru^{II}(bpy)_3]^{2+}$ excited state, which is formed upon excitation of $[Ru^{II}(bpy)_3]^{2+}$ at 447 nm (Scheme 2). Remarkably, only 5 mol % of the ruthenium photosensitizer was needed to achieve the complete transformation of **1** to **2**, which is a significantly smaller amount than the 40 mol % $[Ru^{II}(bpy)_3]^{2+}$ used by Nam and Fukuzumi to generate $[Fe^{IV}(O)(N4Py)]^{2+}$ photochemically.[26] The use of low amounts of the ruthenium photosensitizer is an especially appealing strategy because it entails the in situ generation of a strong oxidant—specifically, $[Ru^{III}(bpy)_3]^{3+}$—in catalytic amounts.

Scheme 2. Chemical Reactions Taking Place during the Photocatalytic Generation of 2

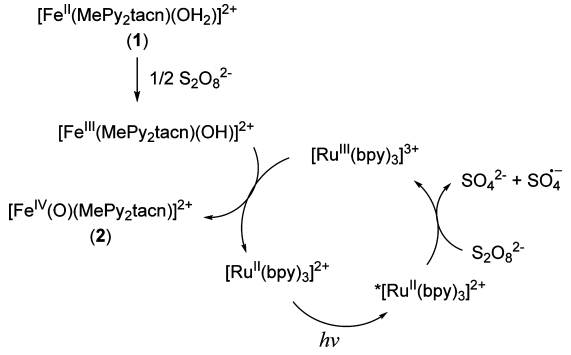

Photoenhanced Oxidation of Sulfides by 2. Under the conditions described above, photocatalytically generated compound **2** reacted with sulfides, as clearly evidenced by the disappearance of the characteristic absorption band of **2** at 715 nm. The rate of the reaction between **2** and an excess of substrate (5 equiv) was obtained by fitting the absorbance at 715 nm over time to a single-exponential decay function. In the absence of irradiation, the observed rate constant (k_{obs}) for the reaction of photochemically generated **2** (0.4 mM **1**, 0.02 mM $[Ru^{II}(bpy)_3]Cl_2$, 4 mM $Na_2S_2O_8$ in CH_3CN/H_2O 1:3) with 5

dx.doi.org/10.1021/ja412059c | J. Am. Chem. Soc. 2014, 136, 4624–4633

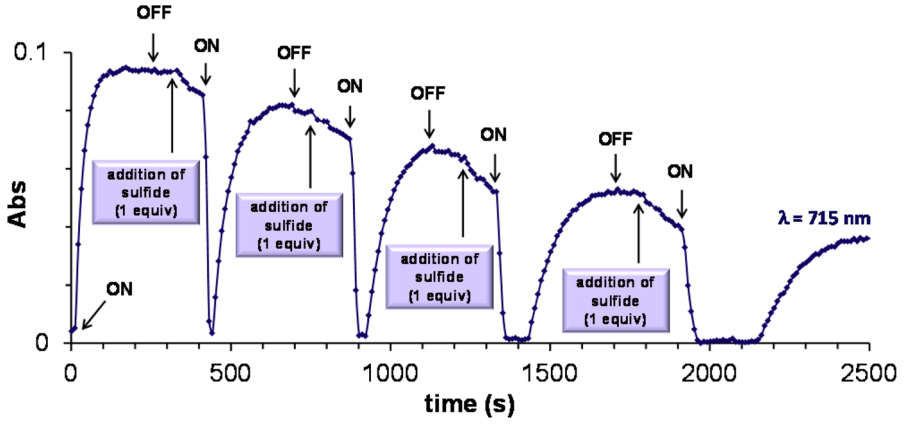

Figure 6. Kinetic trace at 715 nm corresponding to a reaction mixture containing **1** (0.4 mM), 5 mol % $[Ru^{II}(bpy)_3]Cl_2$ (0.02 mM), and $Na_2S_2O_8$ (4 mM, 10 equiv) under N_2 atmosphere at 25 °C. Labels on the figure indicate the initial (ON) and final (OFF) points of irradiation (λ = 447 ± 20 nm) as well as the addition of 1 equiv of ^{MeO}PhSMe.

equiv of 4-methoxythioanisole (^{MeO}PhSMe) was 1.5×10^{-3} s^{-1} at 25 °C. Surprisingly, when the same experiment was carried out under irradiation, the decay of **2** occurred much faster, with k_{obs} = 0.22 s^{-1} (a 150-fold increase with respect to the experiment without irradiation). Indeed, this significant enhancement of the oxygenation rate of the substrate by light deserves special consideration.

Under the photocatalytic conditions described above, compound **2** was regenerated several times after reaction with ^{MeO}PhSMe (Figure 6). Thus, after generating **2**, the irradiation was stopped, and 1 equiv of ^{MeO}PhSMe was added. This initiated a slow decay of the band at 715 nm. Irradiation triggered a much faster oxidation of the substrate, manifested by the immediate and abrupt decay of the characteristic band at 715 nm, which was completely depleted (Figure 6). Under continuous irradiation, once ^{MeO}PhSMe had been consumed, compound **2** was regenerated in ~87% yield, as observed by the recovery of its characteristic absorption at 715 nm (Figure 7).

Such regeneration can be rationalized by considering that the putative iron(II) complex, formed after oxo-transfer to the sulfide, is reoxidized by excess $Na_2S_2O_8$ ($Fe^{II} \rightarrow Fe^{III}$ oxidation) or by the in-situ-photogenerated $[Ru^{III}(bpy)_3]^{3+}$ ($Fe^{II} \rightarrow Fe^{III} \rightarrow Fe^{IV}$) to give **2** again. This process was repeated several times, although the extent of the regeneration decreased with every cycle (see the intensity of the band at 715 nm after each cycle in Figure 6). The reason for this incomplete recovery might be partial decomposition of the iron complex or the photosensitizer, processes usually associated with prolonged irradiation.[33] Interestingly, a delay time between full decay of **2** and the onset of its regeneration was observed after the first cycle, and the extent of this delay increased from cycle to cycle. The origin of the delay was the oxidation of the remaining sulfide not consumed in the initial fast reaction with **2**. Because **2** was increasingly decomposed under photoexcitation from cycle to cycle, the amount of excess sulfide increased accordingly, as did the time needed to accumulate more **2**.

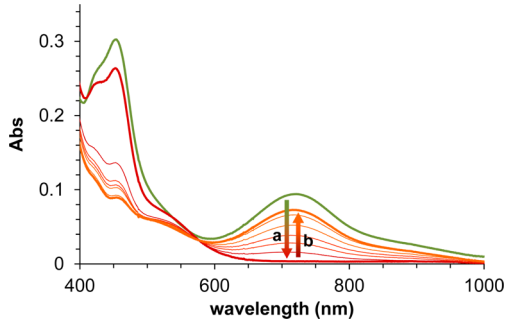

Figure 7. UV/vis spectral changes upon irradiation (447 nm) of a sample of photochemically generated **2** ($[\mathbf{1}]_0$ = 0.4 mM, 5 mol % $[Ru^{II}(bpy)_3]Cl_2$ (0.02 mM), and 10 equiv of $Na_2S_2O_8$ (4 mM)) after addition of 1 equiv of ^{MeO}PhSMe under a N_2 atmosphere at 25 °C in CH_3CN/H_2O 1:3. Step "a" shows the instantaneous decay of compound **2** upon irradiation, and step "b" shows the progressive regeneration of **2** (up to 87%) once the sulfide substrate has been consumed (spectra were recorded every 10 s).

The rate enhancement observed upon light irradiation is remarkable and unprecedented and prompted us to explore the origin of the increase in reactivity. Because the photocatalytic generation of compound **2** takes place in a complex reaction mixture containing several components ($Na_2S_2O_8$, $[Ru(bpy)_3]^{n+}$, sulfide, and iron complex), a simplification of the system was necessary to shed some light on the origin of this phenomenon.

Photoenhanced Reactivity of 2 in Oxygen-Atom Transfer to Sulfides Induced by a Photosensitizer. To gain insight into the origin of the rate enhancement upon light irradiation, we simplified the system by eliminating $Na_2S_2O_8$ from the reaction mixture. This is convenient not only to reduce the number of variables but also because it is well-known that under photoirradiation, $[Ru^{II}(bpy)_3]^{2+}$ acts as a noninnocent oxidative quencher that generates high energy sulfate radicals ($E^0(SO_4^{\bullet -})$ = 2.0 V) from $S_2O_8^{2-}$.[34] Therefore, we studied the capacity of compound **2** (chemically generated by reaction of **1** with PhIO in CH_3CN/H_2O 1:3) to oxidize sulfides under a range of conditions: (i) with/without irradiation and/or (ii) in the presence/absence of the photosensitizer (Table 1). The rate of the direct reaction of **2** (0.4 mM) with 5 equiv of ^{MeO}PhSMe (2 mM) (k_{obs} = 11 ± 1 × 10^{-4} s^{-1}) was unaffected by irradiation at 447 nm (entries 1 and 2). In sharp contrast, the presence of 5 mol % of $[Ru^{II}(bpy)_3]^{2+}$ (0.02 mM) accelerates the decay of **2** 7-fold under irradiation (entries 3 and 4, SI Figure S11). Control experiments showed that in the absence of the sulfide, the decay of **2** also occurred faster under irradiation in the presence of $[Ru^{II}(bpy)_3]^{2+}$ (entries 5 and 6). The effect of light on the self-decay rate (without the sulfide substrate or photosensitizer)

dx.doi.org/10.1021/ja412059c | J. Am. Chem. Soc. 2014, 136, 4624−4633

Table 1. Measured k_{obs} Values Corresponding to the Decay Rate of Chemically Generated 2 (0.4 mM in CH_3CN/H_2O 1:3 in a N_2 Atmosphere at 25°C) under Different Reaction Conditions

entry	^{X}PhSMe (equiv)[a]	$[Ru^{II}(bpy)_3]^{2+}$ (mol %)[b]	light[c]	k_{obs} (10^{-4} s^{-1})[d] X = MeO	k_{obs} (10^{-4} s^{-1})[d] X = CN
1	5		no	11 (±1)	2 (±0.1)
2	5		yes	12 (±1)	3 (±1)
3	5	5	no	12 (±3)	3 (±2)
4	5	5	yes	76 (±6)	28 (±1)
5		5	no	3 (±1)	3 (±1)
6		5	yes	22 (±4)	22 (±4)
7			no	0.9 (±0.2)	0.9 (±0.2)
8			yes	4 (±1)	4 (±1)

[a]Addition of 5 equiv *para*-X-phenylmethylsulfide (^{X}PhSMe, 2 mM) with respect to **2** in the reaction mixture. [b]Addition of 5 mol % $[Ru^{II}(bpy)_3]Cl_2$ (0.02 mM) with respect to **2** in the reaction mixture. [c]Irradiation at 447 nm. [d]k_{obs} values were obtained by fitting the decay of the absorbance at 715 nm over time to a single exponential function.

is minor, albeit significant (entries 7 and 8). From this set of experiments, it is clear that the combination of $[Ru^{II}(bpy)_3]^{2+}$ and irradiation was crucial for the enhanced oxidation rate of ^{MeO}PhSMe by **2**; that is, $[Ru^{II}(bpy)_3]^{2+}$ acts as a photosensitizer, accelerating the process.

Apart from ^{MeO}PhSMe, the photosensitized oxidation of other para-substituted thioanisoles (^{X}PhSMe, X = Me, H, and Cl) was also considerably faster under irradiation and gave ~40% yield of the corresponding sulfoxide in all cases (SI Table S6). The UV/vis absorption spectrum at the end of the reaction did not show the characteristic band of **1** at 414 nm, indicating that **2** did not revert to the starting iron(II) after the oxygen-atom transfer reaction. Instead, ESI-MS spectra evidenced the formation of iron(III)-hydroxo species with major peaks at m/z 547.11 and 199.09 corresponding to $\{[Fe^{III}(OH)(MePy_2tacn)](OTf)\}^+$ and $\{[Fe^{III}(OH)(MePy_2tacn)]\}^{2+}$ (SI Figure S12). Addition of 1 equiv of ascorbic acid (with respect to iron) at the end of the reaction further confirmed this result because more than 75% of **1** was regenerated, as ascertained by the formation of the characteristic band of **1** at 414 nm (SI Figure S13).

Because photochemical and redox processes associated with $[Ru^{II}(bpy)_3]^{2+}$ and iron(IV)-oxo species are rich and varied,[27,33,35,36] several mechanisms can be postulated to rationalize the observed photoenhanced oxygen-atom transferability of **2** (Scheme 3). Some reaction pathways can be discarded on the basis of thermodynamic considerations (Scheme 4). An electron transfer from **2** or ^{MeO}PhSMe to $*[Ru^{II}(bpy)_3]^{2+}$ is not plausible on the basis of the redox potentials of the $*[Ru^{II}(bpy)_3]^{2+}/[Ru^{I}(bpy)_3]^{+}$ (E = +0.84 V vs SCE),[33] $Fe^{V}(O)/Fe^{IV}(O)$ (estimated to be E > 1.5 V by DFT calculations, unpublished results), and $^{MeO}PhSMe^{\bullet+}/^{MeO}$PhSMe ($E$ = +1.13 V vs SCE)[37] couples. Likewise, electron transfer from $*[Ru^{II}(bpy)_3]^{2+}$ to ^{MeO}PhSMe can be discarded if the highly negative reduction potential of this compound is taken into account. Thus, the two most plausible mechanisms would be (Scheme 3) (i) energy transfer from $*[Ru^{II}(bpy)_3]^{2+}$ to **2** to give a highly reactive ***2** and (ii) an electron-transfer from $*[Ru^{II}(bpy)_3]^{2+}$ to compound **2**, resulting in the formation of $[Ru^{III}(bpy)_3]^{3+}$, which would subsequently oxidize ^{MeO}PhSMe to the sulfide radical cation ($^{MeO}PhSMe^{\bullet+}$).

Scheme 3. Mechanistic Pathways to Explain the Rate Enhancement in the Oxidation of Sulfides by 2 under Light Irradiation

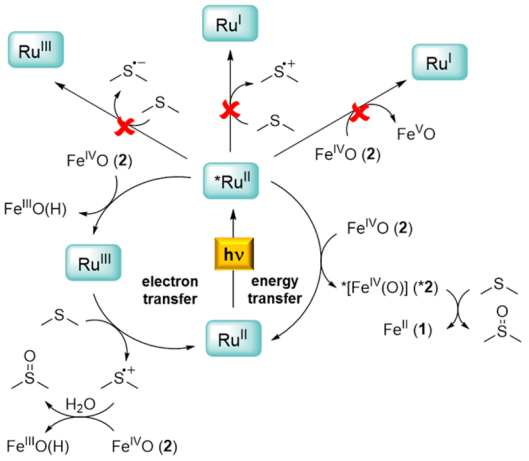

Scheme 4. Redox Potentials of $[Ru(bpy)_3]^{2+/3+}$[a]

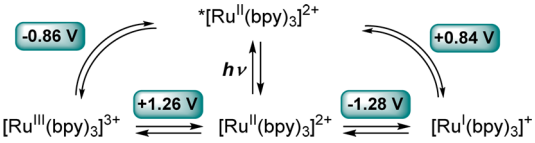

[a] Values vs SCE in CH_3CN.[33]

The rates of reaction of **2** with a series of ^{X}PhSMe (X = OMe, Me, H, and Cl) were studied in the presence of $[Ru^{II}(bpy)_3]^{2+}$ (5 mol %, 0.02 mM) under irradiation at 447 nm to gain further information regarding the mechanism of the photoenhancement of the oxidation rates. As indicated by the small slope of the Hammett plot (ρ = −0.09) represented in SI Figure S14b, the reaction rates are not much influenced by the electron-withdrawing or electron-donating abilities of the para substituents of the sulfide; thus, the electronic properties of the substrate do not affect the rate-determining step of the process.[38] These data are in agreement with the fact that the steady-state $[Ru^{II}(bpy)_3]^{2+}$ concentration was unchanged during the reaction because the intensity of its characteristic absorption band at 450 nm remained stable during the reaction, thus suggesting that the rate-determining step occurred just after the transformation of the photosensitizer and prior to the involvement of the substrate. In sharp contrast, when the Hammett plot was determined from intermolecular competition experiments of *p*-X-thioanisoles versus thioanisole, by plotting the relative amounts of sulfoxide products formed (SI Figure S14c), a ρ value of −2.5 was obtained. This result indicates that the electronic properties of the substrate have a very significant influence in the product-determining step, but this step is not rate-determining.[39] Plotting these values against the one-electron oxidation potentials (E^0_{ox}) of the sulfides gives a linear correlation with a slope of −5.0 (SI Figure S15), a value significantly below the typical values reported for oxygen-atom transfer processes (between −2 and −3)[17,37,40] but somewhat above those obtained for processes involving an electron transfer mechanism (between −8 and −10).[37]

Nanosecond time-resolved absorption spectroscopy (Nd:YAG, 532 nm, 10 ns pulse) was employed to gain insight into the mechanism. Pulsed excitation at 532 nm (15 mJ/pulse) of deaerated CH_3CN/H_2O (1:3) solutions of $[Ru^{II}(bpy)_3]^{2+}$

dx.doi.org/10.1021/ja412059c | J. Am. Chem. Soc. 2014, 136, 4624−4633

(0.07 mM, absorbance 0.06 at 532 nm) led to the disappearance of the latter, as evidenced by the strong bleaching near 470 nm. This was accompanied by the formation of $*[Ru^{II}(bpy)_3]^{2+}$ (^{3}MLCT state), which exhibits characteristic absorption bands below 400 nm and an emission centered at ~620 nm, with a lifetime, τ, of 920 ns (SI Figure S16). As expected, the bleaching at ~470 nm recovered fully in <3 μs (Figure 8 curve a), which is associated with the full

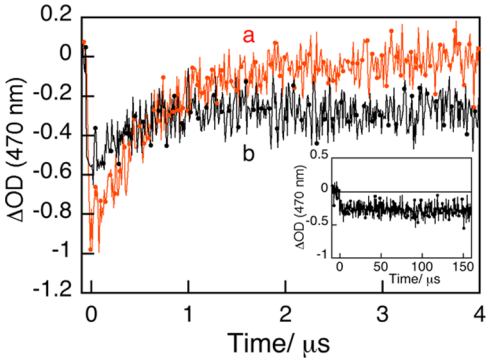

Figure 8. Transient kinetic trace observed at 470 nm after laser flash photolysis (532 nm) of deaerated solution of $[Ru^{II}(bpy)_3]^{2+}$ (0.07 mM) in CH_3CN/H_2O (1:3) (a) in the absence and (b) in the presence of **2** (3.4 mM). Inset: $[Ru^{II}(bpy)_3]^{2+}$ time profile monitored at 470 nm in the presence of **2** (3.4 mM) over a period of 160 μs.

recovery of $[Ru^{II}(bpy)_3]^{2+}$. Comparatively, the same experiment in the presence of increasing amounts of **2** showed that **2** quenched the emission of $*[Ru^{II}(bpy)_3]^{2+}$ at 620 nm with a rate constant, k_q, of 5.7×10^8 M^{-1} s^{-1} (Stern–Volmer plot, SI Figure S17). This is indicative of an interaction between $*[Ru^{II}(bpy)_3]^{2+}$ and **2**. However, under these conditions, $*[Ru^{II}(bpy)_3]^{2+}$ did not completely revert back to the starting $[Ru^{II}(bpy)_3]^{2+}$ compound; that is, its characteristic absorption at 470 nm was not fully recovered. This prolonged bleaching (no changes were detected, even after 150 μs of the laser pulse) (curve b and inset in Figure 8, SI Figure S18) is in accordance with the formation of a new long-lived species with an absorbance in this region lower than that of $[Ru^{II}(bpy)_3]^{2+}$. This new species could be $[Ru^{III}(bpy)_3]^{3+}$, whose absorption at 470 nm is only 4% that of $[Ru^{II}(bpy)_3]^{2+}$ (SI Figure S9). Interestingly, the 470 nm band was completely recovered when the $[Ru^{II}(bpy)_3]^{2+}$/**2** mixture was excited in the presence of ^{MeO}PhSMe (3.4 mM) (Figure 9A). In this case, formation of a species with an absorption band centered at 580 nm was detected (Figure 9B inset). This species can be assigned to a ^{MeO}PhSMe radical cation ($^{MeO}PhSMe^{\bullet+}$)[41,42] formed by oxidation of ^{MeO}PhSMe with the in-situ-generated $[Ru^{III}(bpy)_3]^{3+}$. Indeed, formation of $^{MeO}PhSMe^{\bullet+}$ by in-situ-generated $[Ru^{III}(bpy)_3]^{3+}$ was confirmed by laser excitation at 532 nm of a $[Ru^{II}(bpy)_3]^{2+}/Na_2S_2O_8/^{MeO}$PhSMe mixture (SI Figure S20). Taken together, the data suggest that the photoenhanced oxidation of ^{MeO}PhSMe with **2** occurs through the electron-transfer mechanism depicted in Scheme 3.

To identify the species responsible for the final $1e^-$ oxidation of $^{MeO}PhSMe^{\bullet+}$ to give the observed sulfoxide product, we monitored the UV/vis spectral changes occurring upon addition of ^{MeO}PhSMe (5 equiv) to a mixture containing **2** and $[Ru^{III}(bpy)_3]^{3+}$ (5 equiv). Interestingly, compound **2** was immediately consumed upon substrate addition, even though $[Ru^{III}(bpy)_3]^{3+}$ can generate **2** by oxidation of its iron(II) or

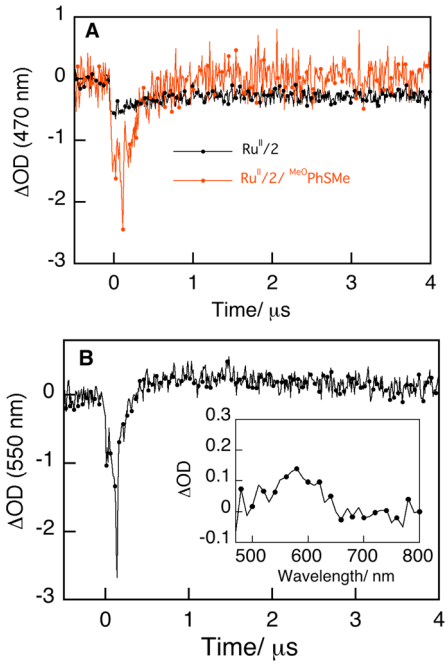

Figure 9. (A) Transient kinetic traces monitored at 470 nm after laser flash photolysis (532 nm) of a deaerated CH_3CN/H_2O (1:3) solution of $[Ru^{II}(bpy)_3]^{2+}$ in the presence of **2** (3.4 mM) (black) or **2** (3.4 mM) and ^{MeO}PhSMe (3.4 mM) (red). (B) Transient kinetic traces monitored at 550 nm after laser flash photolysis (532 nm) of a deaerated solution of $[Ru^{II}(bpy)_3]^{2+}$ in CH_3CN/H_2O (1:3) in the presence of **2** (3.4 mM) and ^{MeO}PhSMe (3.4 mM). Inset: transient absorption spectrum of a deaerated solution of $[Ru^{II}(bpy)_3]^{2+}$ in CH_3CN/H_2O (1:3) in the presence of **2** (3.4 mM) and ^{MeO}PhSMe recorded 2 μs after laser excitation (532 nm).

iron(III) precursors (Figure 7). Thus, under these conditions, $[Ru^{III}(bpy)_3]^{3+}$ reacts instantaneously with ^{MeO}PhSMe to produce $^{MeO}PhSMe^{\bullet+}$, which, in turn, gets immediately oxidized by **2** to give the corresponding sulfoxide and the iron(III)-hydroxo compound. This experiment, together with the results from laser-pulse time-resolved absorption spectroscopy, indicates that compound **2** serves as a $1e^-$ oxidant of both $*[Ru^{II}(bpy)_3]^{2+}$ and $^{MeO}PhSMe^{\bullet+}$ so that the oxidation of 1 equiv sulfide to the corresponding sulfoxide requires 2 equiv of **2** (Scheme 3). This electron transfer mechanism rationalizes the observed exclusive presence of iron(III) at the end of the reaction and the low yield of sulfoxide product (~40%) observed for ^{X}PhSMe (X = OMe, Me, H, and Cl) (see above).

p-Cyanothioanisole (^{CN}PhSMe) constitutes a limiting case for the photocatalyzed electron transfer because its redox potential to form the radical cation (1.61 V) is significantly higher than the oxidation potential of $[Ru^{III}(bpy)_3]^{3+}$ (1.26 V), and therefore, the photoenhanced oxidation of this sulfide by an electron transfer mechanism would be unlikely or it would occur with very low efficiency. As expected, time-resolved absorption spectroscopic studies performed in $[Ru^{II}(bpy)_3]^{2+}$/**2** mixtures in the presence of ^{CN}PhSMe led neither to the full recovery of the absorption at 470 nm nor to the detection of the ^{CN}PhSMe radical cation (SI Figure S21) in the time scale of our laser experiment. These observations indicate that, as expected, the electron transfer from $[Ru^{III}(bpy)_3]^{3+}$ to ^{CN}PhSMe is not taking place. Interestingly, the photoenhanced decay of **2** in the presence of $[Ru^{II}(bpy)_3]^{2+}$ is slightly accelerated with ^{CN}PhSMe (compare entries 4 and 6 in Table

dx.doi.org/10.1021/ja412059c | J. Am. Chem. Soc. 2014, 136, 4624–4633

1) and the sulfoxide yield is low (~10−12%). Given the fact that electron transfer with ^{CN}PhSMe is not operative, an energy transfer mechanism is proposed to explain the moderate rate acceleration and the formation of sulfoxide. This would involve the formation of the ***2** excited state by energy transfer from $*[Ru^{II}(bpy)_3]^{2+}$ to **2** (Scheme 3). Formation of ***2** could also be at the origin of the accelerated decay of **2** with the photosensitizer in the absence of substrate. However, time-resolved absorption measurements failed to detect ***2**. Under our photochemical conditions, excitation of $[Ru^{II}(bpy)_3]^{2+}$/**2** mixtures either at 532 nm or at 355 nm did not provide any transient absorption or emission that could be attributed to ***2**.[43]

In conclusion, in this work, we demonstrate that $[Ru^{II}(bpy)_3]^{2+}$ can photochemically enhance the reaction of an S = 1 oxoiron(IV) complex toward ^{X}PhSMe (X = OCH_3, CH_3, H, and Cl). Nanosecond time-resolved absorption spectroscopic results strongly support an electron transfer from $*[Ru^{II}(bpy)_3]^{2+}$ to **2** to generate $[Ru^{III}(bpy)_3]^{3+}$ and iron(III)-hydroxo complexes. Subsequently, $[Ru^{III}(bpy)_3]^{3+}$ would oxidize the sulfide to its corresponding radical cation, which would react with **2** to form the sulfoxide. At the same time, nanosecond time-resolved absorption data suggest that the photosensitized rate enhancement observed for ^{CN}PhSMe is unlikely to occur through an electron-transfer mechanism. For this reason, we propose that partial contribution of the energy transfer mechanism from $*[Ru^{II}(bpy)_3]^{2+}$ to **2** to give rise to the ***2** excited state could be relevant for this substrate, and it could explain the low amounts of oxidized product detected. This excitation would presumably involve population of a low-lying, more reactive S = 2 excited state. This light-induced low-spin/high-spin transition is reasonable because this process is already well-documented for d^4−d^7 metal complexes.[44] Ongoing experiments to further clarify this mechanism are currently under examination.

Further exploration of the photochemical reactivity of the iron(IV)-oxo complexes, the mechanism of activation, and expansion of this phenomenon toward the reactivity of other substrates are currently being explored.

EXPERIMENTAL SECTION

Materials. Reagents were purchased from commercial sources and used as received without any further purification. Compounds methyl *p*-tolyl sulfide, 4-chlorothioanisole, and formaldehyde were purchased from Fluorochem, Alfa Aesar, and Scharlab, respectively; the rest of the compounds were purchased from Sigma-Aldrich. Solvents were purchased from SDS and Scharlab, purified and dried by passing through an activated alumina purification system (MBraun SPS-800), and stored in an anaerobic glovebox under N_2. Preparation of 1,4-bis(2-pyridylmethyl)-1,4,7-triazacyclononane,[45] Me_2Py_2tacn,[46] and $[Fe^{IV}(O)(Me_2Py_2tacn)]^{2+}$ (**3**)[27] were carried out as previously described. Water (18.2 MΩ·cm) was purified with a Milli-Q Millipore Gradient AIS system.

Physical Methods. UV/vis/NIR spectra were recorded on an Agilent 8453 diode array spectrophotometer (190−1100 nm range) in 1 cm quartz cells. Cyclic voltammetry was recorded using a CH Instruments CHI760c bipotentiostat at room temperature. A cryostat from Unisoku Scientific Instruments was used for the temperature control. Electrospray ionization mass spectrometry (ESI-MS) experiments were performed on a Bruker Daltonics Esquire 6000 Spectrometer. Elemental analyses were conducted in a Carlo Erba Instrument, model CHNS 1108. Crystals of **1** were used for low temperature (100(2) K) X-ray structure determination. The measurement was carried out on a Bruker Smart APEX CCD diffractometer using graphite-monochromated Mo Kα radiation (λ = 0.71073 Å) from an X-ray tube. The measurements were made in the range 2.11−28.64° for θ. Full-sphere data collection was carried out with ω and φ scans. A total of 45423 reflections were collected, of which 14395 [R(int) = 0.0750] were unique. Programs used: data collection, Smart version 5.631 (Bruker AXS 1997-02); data reduction, Saint + version 6.36A (Bruker AXS 2001); absorption correction, SADABS version 2.10 (Bruker AXS 2001).

Structure solution and refinement was performed using SHELXTL Version 6.14 (Bruker AXS 2000−2003). The structure was solved by direct methods and refined by full-matrix least-squares methods on F^2. The non-hydrogen atoms were refined anisotropically. The H-atoms were placed in geometrically optimized positions and forced to ride on the atom to which they are attached. Laser flash photolysis experiments were carried out with the second harmonic (532 nm) of a Q-switched Nd:YAG laser (Spectra Physics QuantaRay (Indi); pulse width ~ 9 ns and 15 mJ pulse^{-1}). The signal from the monochromator/photomultiplier detection system was captured by a Tektronix TDS640A digitizer and transferred to a PC computer that controlled the experiment and provided suitable processing and data storage capabilities.

^{1}H and ^{13}C NMR spectra were recorded on a Bruker Avance 400 MHz spectrometer as solutions at 25 °C and referenced to residual solvent peaks. GC product analyses were performed on an Agilent 7820A gas chromatograph equipped with a HP-5 capillary column 30m × 0.32 mm × 0.25 μm and a flame ionization detector. EPR spectra were recorded on an X-band Bruker EMX spectrometer equipped with an Oxford Instruments ESR-900 continuous-flow helium cryostat and an ER-4116 DM Bruker cavity. ^{57}Fe Mössbauer experiments were performed at 80 K on a zero-field Mössbauer spectrometer equipped with a Janis SVT-400 cryostat as already described.[47] Analysis of the data was performed with the program WMOSS (WEB Research, Edina, MN, USA).

Fe K-edge X-ray absorption spectra were collected on beamline 9-3 of the Stanford Synchrotron Radiation Lightsource (SSRL) at the SLAC National Accelerator Laboratory with a SPEAR storage ring current of ~450 mA at a power of 3.0 GeV. The incoming X-rays were unfocused using a Si(220) double crystal monochromator, which was detuned to 40% of the maximal flux to attenuate harmonic X-rays. Four (4) scans were collected from 6882 to 8000 eV at a temperature (10 K) that was controlled by an Oxford Instruments CF1208 continuous flow liquid helium cryostat. Harmonic rejection was achieved by a 9 keV cutoff filter. Data were obtained as fluorescence excitation spectra with a 100-element solid-state Ge detector array (Canberra). In fluorescence mode, photon scattering "noise" was reduced using a 3 μm Mn filter and a Soller slit. An iron foil was placed in the beam pathway prior to I_0 and scanned concomitantly for an energy calibration, with the first inflection point of the edge assigned to 7112.0 eV. Photoreduction was monitored by scanning the same spot on the sample twice and comparing the first derivative peaks associated with the edge energy during collection, but none was observed in the present study. The detector channels from the scans were examined, calibrated, averaged, and processed for EXAFS analysis using EXAFSPAK to extract $\chi(k)$.

Theoretical phase and amplitude parameters for a given absorber−scatterer pair were calculated using FEFF 8.40 and were utilized by the "opt" program of the EXAFSPAK package during curve fitting. Parameters for **2** were calculated using similar coordinates of the available crystal structure of the corresponding Fe^{II} complex (**1**). In all analyses, the coordination number of a given shell was a fixed parameter and was varied iteratively in integer steps while the bond lengths (R) and mean-square deviation (σ^2) were allowed to freely float. The amplitude reduction factor, S_0, was fixed at 0.9 while the edge-shift parameter E_0 was allowed to float as a single value for all shells. Thus, in any given fit, the number of floating parameters was typically equal to (2 × number of shells) + 1. Pre-edge analysis was performed on data normalized in the "process" program of the EXAFSPAK package, and pre-edge features were fit between 7108 and 7118 eV using the Fityk program with pseudo-Voigt functions composed of 50:50 Gaussian/Lorentzian functions.

dx.doi.org/10.1021/ja412059c | J. Am. Chem. Soc. 2014, 136, 4624−4633

Synthesis of *N*-Methyl-*N*′,*N*″-bis(2-pyridylmethyl)-1,4,7-triazacyclononane ($MePy_2tacn$). 1,4-Bis(2-pyridylmethyl)-1,4,7-triazacyclononane (0.34 g, 1.09 mmol) was dissolved in formaldehyde 37% (3 mL), 98% formic acid (3 mL), and water (2.5 mL), and the resulting yellow solution was refluxed for 30 h. After cooling to room temperature, 3 mL of HCl was added, and the mixture was left stirring for 10 min. The solvent was removed under vacuum, and a small amount of water (10 mL) was added to the resulting residue. The solution was brought to pH 14 by the addition of NaOH (4 M). After stirring for 20 min, the aqueous phase was extracted with CH_2Cl_2 (3 × 50 mL). The combined organic phases were dried over anhydrous $MgSO_4$, and the solvent was removed under reduced pressure. The resulting residue was treated with *n*-hexane (75 mL) and stirred for 12 h. The solvent was decanted and removed under reduced pressure to yield 0.162 g of a colorless oil (0.50 mmol, 46%). ^{1}H NMR ($CDCl_3$, 300 MHz, 300 K) δ, ppm: 8.50 (d, 2H, Py$\mathbf{H}_\alpha$), 7.64 (dt, 2H, Py$\mathbf{H}_\gamma$), 7.49 (d, 2H, Py$\mathbf{H}_\beta$), 7.10 (dd, 2H, Py$\mathbf{H}_{\beta'}$), 3.82 (s, 4H, C$\mathbf{H}_2$-Py), 2.90−2.82 (m, 8H, N−C$\mathbf{H}_2$), 2.74 (s, 4H, N−C$\mathbf{H}_2$), 2.34 (s, 3H, C$\mathbf{H}_3$). The analysis is consistent with the previously reported synthesis of $MePy_2tacn$.[48]

Synthesis of $[Fe^{II}(CH_3CN)(MePy_2tacn)](OTf)_2$ (1). To a vial containing $MePy_2tacn$ (150 mg, 0.46 mmol) dissolved in THF (1 mL) was added dropwise a THF solution (1 mL) of $Fe(CH_3CN)_2(CF_3SO_3)_2$ (200 mg, 0.46 mmol). After stirring for 3 h, the resulting red solid was filtered, washed with Et_2O (3 × 2 mL), and dried under vacuum. Recrystallization of the red solid by Et_2O diffusion into a saturated CH_2Cl_2/CH_3CN solution yielded dark red single crystals (198 mg, 60%) suitable for diffraction analysis. ^{1}H NMR (CD_3CN, 400 MHz, 273 K) δ, ppm: 8.90 (d, J = 5.6 Hz, 1H, Py**H**), 7.94 (td, J = 7.6 Hz, J' = 1.2 Hz, 1H, Py**H**), 7.81 (td, J = 7.6 Hz, J' = 1.2 Hz, 1H, Py**H**), 7.61 (d, J = 7.6 Hz, 1H, Py**H**), 7.56 (t, J = 6.6 Hz, 1H, Py**H**), 7.52 (d, J = 7.6 Hz, 1H, Py**H**), 7.29 (d, J = 5.2 Hz, 1H, Py**H**), 7.18 (t, J = 6.4 Hz, 1H, Py**H**), 4.72 (d, J = 16 Hz, 1H, C$\mathbf{H}_2$-Py), 4.58 (d, J = 15.6 Hz, 1H, C$\mathbf{H}_2$Py), 4.54 (d, J = 16 Hz, 1H, C$\mathbf{H}_2$Py), 4.06 (d, J = 16.4 Hz, 1H, C$\mathbf{H}_2$Py), 3.5−2.9 (m, 10H, N−C$\mathbf{H}_2$), 2.60−2.59 (m, 1H, N−C$\mathbf{H}_2$), 2.59 (s, 3H, C$\mathbf{H}_3$), 1.61 (td, J = 13.2 Hz, J' = 6.4 Hz, 1H, N−C$\mathbf{H}_2$). ^{13}C NMR (CD_3CN, 100 MHz, 273 K) δ, ppm: 166.07, Py**C**), 166.03 (1C, Py**C**), 157.42 (1C, Py**C**), 154.39 (1C, Py**C**), 137.57 (1C, Py**C**), 137.42 (1C, Py**C**), 125.09 (1C, Py**C**), 125.06 (1C, Py**C**), 122.60 (1C, Py**C**), 122.15 (1C, Py**C**), 68.07 (1C, Py-**C**H_2), 67.01 (1C, Py-**C**H_2), 61.05 (1C, N-**C**H_2), 60.38 (1C, N-**C**H_2), 60.18 (2C, N-**C**H_2), 59.01(1C, N-**C**H_2), 58.20 (1C, N-**C**H_2), 49.38 (1C, **C**H_3). ESI-MS (m/z): $[M - CH_3CN - CF_3SO_3]^+$ = 530.2 (100%), $[M - CH_3CN - 2CF_3SO_3]^{2+}$ = 190.5 (26%). Anal. Calcd. (%) for $C_{23}H_{30}F_6FeN_6O_6S_2 \cdot 1/2H_2O$ (729.43): C, 37.87; H, 4.28; N, 11.52; S, 8.79. Found: C, 37.99; H, 4.31; H, 11.41; S, 8.67.

Preparation of $[Fe^{IV}(O)(MePy_2tacn)]^{2+}$ (2) with PhIO. In an anaerobic glovebox, **1** (2.3 mg, 3.9 × 10^{-3} mmol) and PhIO (14 mg, 6.4 × 10^{-2} mmol) were mixed in CH_3CN (2 mL). The resulting solution was vigorously stirred 10−12 min. Removal of unreacted PhIO was achieved by filtration, which afforded a pale green solution of compound **2**. The yield of the reaction was estimated according to the amount of Fe^{IV} determined by Mössbauer spectroscopy by preparation of a 50% ^{57}Fe-enriched sample of compound **2**. Yield: 82%. ^{1}H NMR (CD_3CN, 400 MHz, 300 K) δ, ppm: 46.46 (s, 1H, Py$\mathbf{H}_\beta$), 13.34 (s, 1H, Py$\mathbf{H}_\gamma$), 11.22 (s, 1H, Py$\mathbf{H}_\gamma$), 2.05 (s, 1H, Py$\mathbf{H}_\beta$), −1.36 (s, 1H, Py$\mathbf{H}_\beta$), −13.27 (s, 1H, Py$\mathbf{H}_\beta$). ESI-MS (m/z): $[M - CF_3SO_3]^+$ = 546.1 (100%), $[M - 2CF_3SO_3]^{2+}$ = 198.5 (5%). UV/vis (CH_3CN/H_2O 1:3): λ_{max} = 715 nm, ε = 240 M^{-1} cm^{-1}

Preparation of $[Fe^{IV}(O)(MePy_2tacn)]^{2+}$ (2) under Photocatalytic Conditions. In an anaerobic glovebox, a solution of **1** (0.72 mg, 1 × 10^{-3} mmol) in CH_3CN (625 μL) was placed in a UV/vis cuvette. Addition of 5 mol % of $[Ru(bpy)_3]Cl_2$ (0.05 μmol, 100 μL of a 0.5 mM solution in deaerated water), 10 equiv of $Na_2S_2O_8$ (10 μmol, 100 μL of a 100 mM solution in deaerated water), and deaerated water (1.6 mL) afforded the initial reaction mixture (solvent ratio CH_3CN/H_2O 1:3, 0.4 mM in **1**). Irradiation at 447 nm caused immediate changes in the UV/vis spectrum that led to the formation of **2**, as evidenced by the appearance of its characteristic band at 715 nm (see Figure 5).

Kinetic Studies. The required amount of **2** (625 μL of a 1.6 mM solution of **2** in CH_3CN obtained by direct oxidation of **1** with PhIO) was diluted in deaerated Milli-Q water (1.67 mL), then the desired quantity of photosensitizer (dissolved in CH_3CN:H_2O 1:3) and/or sulfide (^{X}PhSMe, dissolved in CH_3CN) was added. Finally, the appropriate amounts of CH_3CN and H_2O were added to reach a CH_3CN/H_2O ratio of 1:3 and an initial concentration of **2** of 0.4 mM. The progress of the reaction was monitored by UV/vis spectroscopy at 25 °C.

Identification and Quantification of Sulfoxides. Reaction of **2** with sulfides (^{X}PhSMe) caused a decay of its characteristic absorption band (λ_{max} = 715 nm). After full decay of this band, an internal standard was added to the solution (trimethoxybenze or biphenyl), and the amount of formed sulfoxide was quantified by ^{1}H NMR spectroscopy or gas chromatography.

■ ASSOCIATED CONTENT

Supporting Information

NMR and Mössbauer spectra of **1**, EPR and Mössbauer spectra of $[Fe^{III}(OH)(MePy_2tacn)](OTf)_2$, NMR spectrum of **2**, UV/vis control experiments, quantification of sulfoxide products, analysis of the final iron species, Hammett plots, and photophysical experiments. This material is available free of charge via the Internet at http://pubs.acs.org.

■ AUTHOR INFORMATION

Corresponding Author

anna.company@udg.edu; miquel.costas@udg.edu; julia.perez@uv.es; julio.lloret@udg.edu

Notes

The authors declare no competing financial interest.

■ ACKNOWLEDGMENTS

We acknowledge the European Commission for projects FP7-PEOPLE-2011-CIG-303522 (A.C.), FP7-PEOPLE-2010-ERG-268445 (J.L.-F.), FP7-PEOPLE-CIG-303522 (M.G.B.), and ERC-009StG-239910 (M.C.); the Spanish Ministry of Science for Projects CTQ2012-37420-C02-01/BQU (M.C.), CSD2010-00065 (M.C.), and CTQ2011-27758 (J.P.P.); Generalitat de Catalunya for an ICREA Academia Award and Project 2009-SGR637 (M.C.); and Generalitat Valenciana for Project ACOMP/2013/008 (J.P.P.). The Spanish Ministry of Science is acknowledged for a Ramón y Cajal contract to A.C. and J.L.-F. J.M.L. acknowledges the support, in part, of Labex ARCANE (ANR-11-LABX-0003-01). The work at the University of Minnesota was supported by the US National Science Foundation (Grant CHE1058248 to L.Q.) and the Dr. Venkateswarlu Pothapragada and Family Fellowship (to M.P.). XAS data were collected at beamline 9-3 of the Stanford Synchrotron Radiation Lightsource supported by the US-NIH and US-DOE. We thank Catexel for a generous gift of tritosyl-1,4,7-triazacyclononane.

■ REFERENCES

(1) Costas, M.; Mehn, M. P.; Jensen, M. P.; Que, L., Jr. *Chem. Rev.* **2004**, *104*, 939.

(2) Gómez, L.; Garcia-Bosch, I.; Company, A.; Benet-Buchholz, J.; Polo, A.; Sala, X.; Ribas, X.; Costas, M. *Angew. Chem., Int. Ed.* **2009**, *48*, 5720.

(3) Chen, M. S.; White, M. C. *Science* **2007**, *318*, 783.

(4) Chen, M. S.; White, M. C. *Science* **2010**, *327*, 566.

(5) Garcia-Bosch, I.; Codola, Z.; Prat, I.; Ribas, X.; Lloret-Fillol, J.; Costas, M. *Chem.—Eur. J.* **2012**, *18*, 13269.

(6) Codola, Z.; Garcia-Bosch, I.; Acuna-Pares, F.; Prat, I.; Luis, J. M.; Costas, M.; Lloret-Fillol, J. *Chem.—Eur. J.* **2013**, *19*, 8042.

(7) Lloret-Fillol, J.; Codola, Z.; Garcia-Bosch, I.; Gómez, L.; Jose Pla, J.; Costas, M. *Nat. Chem.* **2011**, *3*, 807.
(8) Price, J. C.; Barr, E. W.; Tirupati, B.; Bollinger, J. M.; Krebs, C. *Biochemistry* **2003**, *42*, 7497.
(9) Proshlyakov, D. A.; Henshaw, T. F.; Monterosso, G. R.; Ryle, M. J.; Hausinger, R. P. *J. Am. Chem. Soc.* **2004**, *126*, 1022.
(10) Eser, B. E.; Barr, E. W.; Frantorn, P. A.; Saleh, L.; Bollinger, J. M., Jr.; Krebs, C.; Fitzpatrick, P. F. *J. Am. Chem. Soc.* **2007**, *129*, 11334.
(11) Hoffart, L. M.; Barr, E. W.; Guyer, R. B.; Bollinger, J. M., Jr.; Krebs, C. *Proc. Natl. Acad. Sci. U.S.A.* **2006**, *103*, 14738.
(12) Panay, A. J.; Lee, M.; Krebs, C.; Bollinger, J. M., Jr.; Fitzpatrick, P. F. *Biochemistry* **2011**, *50*, 1928.
(13) Que, L., Jr. *Acc. Chem. Res.* **2007**, *40*, 493.
(14) Nam, W. *Acc. Chem. Res.* **2007**, *40*, 522.
(15) Company, A.; Lloret-Fillol, J.; Costas, M. In *Comprehensive Inorganic Chemistry II*; Reedijk, J., Poeppelmeier, K., Eds.; Elsevier: Oxford, 2013; Vol. 3, p 487.
(16) Kaizer, J.; Klinker, E. J.; Oh, N. Y.; Rohde, J. U.; Song, W. J.; Stubna, A.; Kim, J.; Munck, E.; Nam, W.; Que, L., Jr. *J. Am. Chem. Soc.* **2004**, *126*, 472.
(17) Company, A.; Prat, I.; Frisch, J. R.; Mas-Balleste, R.; Gueell, M.; Juhasz, G.; Ribas, X.; Muenck, E.; Luis, J. M.; Que, L., Jr.; Costas, M. *Chem.—Eur. J.* **2011**, *17*, 1622.
(18) Hong, S.; Lee, Y.-M.; Cho, K.-B.; Sundaravel, K.; Cho, J.; Kirn, M. J.; Shin, W.; Nam, W. *J. Am. Chem. Soc.* **2011**, *133*, 11876.
(19) Comba, P.; Fukuzumi, S.; Kotani, H.; Wunderlich, S. *Angew. Chem., Int. Ed.* **2010**, *49*, 2622.
(20) Sastri, C. V.; Lee, J.; Oh, K.; Lee, Y. J.; Lee, J.; Jackson, T. A.; Ray, K.; Hirao, H.; Shin, W.; Halfen, J. A.; Kim, J.; Que, L., Jr.; Shaik, S.; Nam, W. *Proc. Natl. Acad. Sci. U.S.A.* **2007**, *104*, 19181.
(21) England, J.; Guo, Y.; Van Heuvelen, K. M.; Cranswick, M. A.; Rohde, G. T.; Bominaar, E. L.; Muenck, E.; Que, L., Jr. *J. Am. Chem. Soc.* **2011**, *133*, 11880.
(22) Seo, M. S.; Kim, N. H.; Cho, K.-B.; So, J. E.; Park, S. K.; Clemancey, M.; Garcia-Serres, R.; Latour, J.-M.; Shaik, S.; Nam, W. *Chem. Sci.* **2011**, *2*, 1039.
(23) Xue, G.; De Hont, R.; Muenck, E.; Que, L., Jr. *Nat. Chem.* **2010**, *2*, 400.
(24) McDonald, A. R.; Que, L., Jr. *Coord. Chem. Rev.* **2013**, *257*, 414.
(25) Lee, Y.-M.; Dhuri, S. N.; Sawant, S. C.; Cho, J.; Kubo, M.; Ogura, T.; Fukuzumi, S.; Nam, W. *Angew. Chem., Int. Ed.* **2009**, *48*, 1803.
(26) Kotani, H.; Suenobu, T.; Lee, Y.-M.; Nam, W.; Fukuzumi, S. *J. Am. Chem. Soc.* **2011**, *133*, 3249.
(27) Wang, D.; Ray, K.; Collins, M. J.; Farquhar, E. R.; Frisch, J. R.; Gomez, L.; Jackson, T. A.; Kerscher, M.; Waleska, A.; Comba, P.; Costas, M.; Que, L., Jr. *Chem. Sci.* **2013**, *4*, 282.
(28) Prat, I.; Company, A.; Corona, T.; Parella, T.; Ribas, X.; Costas, M. *Inorg. Chem.* **2013**, *52*, 9229.
(29) Diebold, A.; Hagen, K. S. *Inorg. Chem.* **1998**, *37*, 215.
(30) Britovsek, G. J. P.; England, J.; White, A. J. P. *Inorg. Chem.* **2005**, *44*, 8125.
(31) Lim, M. H.; Rohde, J. U.; Stubna, A.; Bukowski, M. R.; Costas, M.; Ho, R. Y. N.; Munck, E.; Nam, W.; Que, L., Jr. *Proc. Natl. Acad. Sci. U.S.A.* **2003**, *100*, 3665.
(32) Klinker, E. J.; Kaizer, J.; Brennessel, W. W.; Woodrum, N. L.; Cramer, C. J.; Que, L., Jr. *Angew. Chem., Int. Ed.* **2005**, *44*, 3690.
(33) Campagna, S.; Puntoriero, F.; Nastasi, F.; Bergamini, G.; Balzani, V. In *Photochemistry and Photophysics of Coordination Compounds I*; Balzani, V., Campagna, S., Eds.; Springer-Verlag Berlin: Heidelberg, 2007.
(34) *CRC Handbook of Chemistry and Physics*; Lide, D. R., Ed.; CRC Press: Boca Raton, FL, 2005.
(35) Lee, Y.-M.; Kotani, H.; Suenobu, T.; Nam, W.; Fukuzumi, S. *J. Am. Chem. Soc.* **2008**, *130*, 434.
(36) Morimoto, Y.; Kotani, H.; Park, J.; Lee, Y.-M.; Nam, W.; Fukuzumi, S. *J. Am. Chem. Soc.* **2010**, *133*, 403.
(37) Goto, Y.; Matsui, T.; Ozaki, S.; Watanabe, Y.; Fukuzumi, S. *J. Am. Chem. Soc.* **1999**, *121*, 9497.
(38) Oh, N. Y.; Suh, Y.; Park, M. J.; Seo, M. S.; Kim, J.; Nam, W. *Angew. Chem., Int. Ed.* **2005**, *44*, 4235.
(39) Simmons, E. M.; Hartwig, J. F. *Angew. Chem., Int. Ed.* **2012**, *51*, 3066.
(40) Sastri, C. V.; Seo, M. S.; Park, M. J.; Kim, K. M.; Nam, W. *Chem. Commun.* **2005**, 1405.
(41) Yokoi, H.; Hatta, A.; Ishiguro, K.; Sawaki, Y. *J. Am. Chem. Soc.* **1998**, *120*, 12728.
(42) Ioele, M.; Steenken, S.; Baciocchi, E. *J. Phys. Chem. A* **1997**, *101*, 2979.
(43) Note: no transient species was detected after laser flash photolysis excitation of compound **2**.
(44) Stock, P.; Pedzinski, T.; Spintig, N.; Grohmann, A.; Hoerner, G. *Chem.—Eur. J.* **2013**, *19*, 839.
(45) McLachlan, G. A.; Fallon, G. D.; Martin, R. L.; Moubaraki, B.; Murray, K. S.; Spiccia, L. *Inorg. Chem.* **1994**, *33*, 4663.
(46) Roelfes, G.; Vrajmasu, V.; Chen, K.; Ho, R. Y. N.; Rohde, J. U.; Zondervan, C.; la Crois, R. M.; Schudde, E. P.; Lutz, M.; Spek, A. L.; Hage, R.; Feringa, B. L.; Munck, E.; Que, L., Jr. *Inorg. Chem.* **2003**, *42*, 2639.
(47) Carboni, M.; Clémancey, M.; Molton, F.; Pécaut, J.; Lebrun, C.; Dubois, L.; Blondin, G.; Latour, J. M. *Inorg. Chem.* **2012**, *51*, 10447.
(48) Dickie, A. J.; Hockless, D. C. R.; Willis, A. C.; McKeon, J. A.; Jackson, W. G. *Inorg. Chem.* **2003**, *42*, 3822.